COMPRESSIVE SENSING BASED SPECULAR MULTIPATH EXPLOITATION FOR THROUGH-THE-WALL RADAR IMAGING

Michael Leigsnering[⋆] *Fauzia Ahmad*[†] *Moeness G. Amin*[†] *Abdelhak M. Zoubir*[⋆]

[⋆]Signal Processing Group, Institute of Telecommunications
Technische Universität Darmstadt, 64283 Darmstadt, Germany

[†]Radar Imaging Laboratory, Center for Advanced Communications
Villanova University, Villanova, PA 19085 USA

ABSTRACT

Multipath propagation can create ghost targets that severely affect the reconstruction quality of through-the-wall radar images. We propose a compressive sensing (CS) based reconstruction method, which inverts a specular multipath model through exploitation of the structured sparsity in the scene. This allows suppression of the ghost targets and increased signal-to-clutter ratio at the target locations, leading to 'clean' images of stationary scenes. Simulation results demonstrate the effectiveness of the proposed approach.

Index Terms— Through-the-wall, Multipath, Compressive Sensing

1. INTRODUCTION

For many civilian and military applications, it is essential to acquire accurate information of scenes behind walls or other opaque obstacles. Through-the-wall radar imaging (TWRI) can provide high-resolution images of otherwise obscured areas utilizing electromagnetic wave propagation [1–5].

We consider two major challenges that affect image quality and applicability of TWRI in practice. First, we address multipath propagation due to specular reflections from interior walls. These additional propagation paths may result in the power being focused at so-called ghost targets, which can be confused with real targets in the image [6]. Earlier work focused on mitigating the effects of multipath propagation [1]. Subsequently, multipath propagation has been exploited in order to gain more target information [7] or enhance the power focused onto the target pixels [6].

Second, the desire for high-resolution images results in large amounts of data to be recorded, stored, and subsequently processed. An efficient data acquisition approach based on compressive sensing (CS) was first proposed in [8]. Subsequent research has proven CS to be a powerful approach to obtain a good image quality from few measurements, provided that the scene is sparse in its canonical or any other basis [8–11]. However, ghost targets due to multipath may render the scene less sparse and, therefore, affect image quality of the reconstruction.

In this paper, we consider the problem of multipath propagation in view of efficient data collection. We combine multipath exploitation [6] with CS for TWRI [8] to obtain a sparse reconstruction of the scene. A specular multipath propagation model, developed by the authors in [12], is employed in two different CS formulations. The first method assumes full knowledge of the target scattering characteristics, which may not be available in practical applications. The second method is based on a group sparse constraint, which achieves scene reconstruction using a mixed-norm optimization approach. Thus, we only need to assume stationary point-like targets. However, we do not require them to be fully isotropic. We obtain a good estimate of the scene, featuring enhanced target strength and suppressed ghost targets. The effectiveness of the proposed methods is demonstrated using simulated data.

The remainder of the paper is organized as follows. Multipath propagation model for the received signal is introduced in Section 2. In Section 3, we describe the proposed CS reconstruction approaches. Section 4 contains simulation results and conclusions are drawn in Section 5.

2. SIGNAL MODEL

The signal model is formulated using a monostatic stepped-frequency approach [1]. The proposed approach, however, is applicable to other TWRI techniques.

Assume that N wideband transceivers are arranged as a line array, with element positions $x_n, n = 0, \ldots, N-1$ at a certain standoff distance from the wall. In the stepped-frequency approach, the wideband pulse is approximated by M monochromatic signals. The frequencies $f_m, m = 0, \ldots, M-1$ are uniformly spaced over the desired bandwidth $f_{M-1} - f_0$. In this work, we consider target returns

The work by F. Ahmad and M. Amin was supported in part by ARO and ARL under contract W911NF-11-1-0536 and in part by ONR under grant N00014-11-1-0576.

only, assuming that the wall response has been properly dealt with using wall clutter mitigation techniques [13–15].

We divide the region of interest into a regular grid of $N_x \times N_y$ points, with N_x and N_y representing the number of points in crossrange and downrange, respectively. Let σ_p be the complex reflectivity of the pth spatial grid point or the pth target, where $p = 0, 1, \ldots, N_x N_y - 1$. Note that the absence of a target at a particular grid point is simply represented by a zero value for the corresponding target reflectivity. Assuming monostatic operation, the target return can be expressed as,

$$y[m,n] = \sum_{p=0}^{N_x N_y - 1} \sigma_p \exp(-j2\pi f_m \tau_{pn}), \qquad (1)$$

where τ_{pn} denotes the round-trip propagation delay between the p-th target and the n-th transceiver. The target reflectivities are assumed constant, independent of frequency and aspect angle. We assume knowledge or accurate estimation of the wall thickness d and permittivity ε_r. For a method to obtain accurate estimates of the wall parameters, refer to [16]. Hence, τ_{pn} can be calculated from geometric considerations [1].

2.1. Vectorized Measurements

The measured data vector $\boldsymbol{y} \in \mathbb{C}^{MN \times 1}$ is obtained by stacking the measurements $y[m,n]$ into a single column vector,

$$\boldsymbol{y} = [y[0,0], \ldots, y[M-1,0], \ldots, y[M-1,N-1]]^T. \quad (2)$$

The complex reflectivities σ_p can be vectorized as,

$$\boldsymbol{s} = [\sigma_0, \sigma_1, \ldots, \sigma_{N_x N_y - 1}]^T. \qquad (3)$$

The dictionary $\boldsymbol{\Phi}$ contains the phase terms of the target model,

$$[\boldsymbol{\Phi}]_{ip} = \exp(-j2\pi f_m \tau_{pn}), \quad m = i(\mathrm{mod}\, M), n = \lfloor i/M \rfloor, \quad i = 0, 1, \ldots, MN-1. \qquad (4)$$

Now, using the above equations, Eq. (1) can be rewritten as

$$\boldsymbol{y} = \boldsymbol{\Phi}\boldsymbol{s}. \qquad (5)$$

2.2. Interior Wall Multipath

In TWRI, multipath propagation corresponds to indirect paths which involve reflections at one or more interior walls, by which the signal may reach the target. The dominant multipath component corresponds to a 'bistatic' scattering scenario. That is, the transmitted signal propagates directly to a scatterer and the scattered wave travels back to the transceiver after being reflected by an interior wall or vice versa. This type of multipath propagation results in ghost targets that lie within the perimeter of the imaged room [6]. Other multipath scenarios exist, but can usually be omitted, since either the resulting ghost target is weak or it lies outside the room and can be mitigated by time-gating.

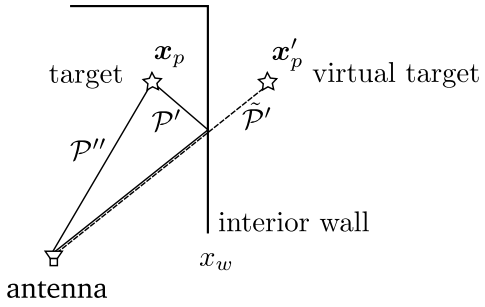

Fig. 1. Multipath via reflection at an internal wall.

Consider the scattering scenario illustrated in Fig. 1, where the front wall has been ignored for simplicity. The pth target is located at $\boldsymbol{x}_p = [x_p, y_p]^T$, and the interior wall is parallel to the y-axis and located at $x = x_w$. Multipath propagation consists of the propagation from the nth antenna to the target along the path $\mathcal{P}''$ and then from the target via a reflection at the interior wall along the path $\mathcal{P}'$. Assuming a specular wall reflection, the geometry can be equivalently expressed by reflecting the target about the interior wall. We obtain a virtual target located at $\boldsymbol{x}'_p = [2x_w - x_p, y_p]^T$ and the delay associated with path $\mathcal{P}'$ is the same as that of the path $\tilde{\mathcal{P}}'$ from the virtual target to the antenna. Hence, we can use the method for determining the delay of the direct path for the calculation of the one-way propagation delay $\tau_{pn}^{(\mathcal{P}')}$ of the multipath. The delay calculation method is described in [1], and utilizes Snell's law and the known front wall parameters.

Having observed the significance and the mechanism of multipath propagation, these observations have to be incorporated into the measurement model (5). We assume a maximum of $K-1$ multipath propagation paths and one direct path. For each considered propagation path k, we use a separate target reflectivity vector $\boldsymbol{s}^{(k)}$, as the target radar cross section (RCS) for bistatic reflection generally differs from the monostatic one. However, we assume that the target reflectivity corresponding to each path is constant across the array elements (see [12] for details on feasibility of this assumption). Hence, (5) can be modified to

$$\boldsymbol{y} = \boldsymbol{\Phi}^{(0)}\boldsymbol{s}^{(0)} + \boldsymbol{\Phi}^{(1)}\boldsymbol{s}^{(1)} + \cdots + \boldsymbol{\Phi}^{(K-1)}\boldsymbol{s}^{(K-1)} \qquad (6)$$

The received multipath components are expressed as the summation of the target reflectivity vectors $\boldsymbol{s}^{(k)}$ multiplied by the respective dictionary $\boldsymbol{\Phi}^{(k)}$. The dictionaries include the modified delays as described above, resulting in phase terms analogous to (4).

Note that, in practice, the number of multipath contributions is limited by the number of large flat surfaces. Thus, for a single room, one would expect $K = 6$ propagation paths: one direct path and 5 multipath propagation paths due to three interior walls, floor, and ceiling.

3. COMPRESSIVE SENSING AND RECONSTRUCTION

The ultimate goal of the proposed approach is to obtain a good representation of the scene, employing an efficient data acquisition scheme. Hence, we aim at obtaining a faithful reconstruction, using as few measurements as possible. First, we define how the considered measurements are selected from the full data vector in (6). For stepped-frequency operation, as considered in this work, a binary downsampling matrix $\boldsymbol{D} \in \{0,1\}^{J \times MN}$ is a reasonable choice [8, 17]. In this case, one can think of $\boldsymbol{D}$ as a fat matrix that randomly selects J entries of $\boldsymbol{y}$, discarding the rest. Hence, we obtain an undersampled measurement vector $\bar{\boldsymbol{y}} = \boldsymbol{D}\boldsymbol{y}$.

Applying undersampling to the model in (6), yields

$$\bar{\boldsymbol{y}} = \boldsymbol{A}^{(0)}\boldsymbol{s}^{(0)} + \boldsymbol{A}^{(1)}\boldsymbol{s}^{(1)} + \cdots + \boldsymbol{A}^{(K-1)}\boldsymbol{s}^{(K-1)}, \quad (7)$$

where $\boldsymbol{A}^{(k)} = \boldsymbol{D}\boldsymbol{\Phi}^{(k)}, k = 0, 1, \ldots, K-1$.

Using the final measurement equation (7), we propose different schemes for sparse reconstruction of the image.

3.1. Simple CS Reconstruction

Assuming all sub-images $\boldsymbol{s}^{(k)}$ to be identical, as in the case of isotropic scatterers such as spheres, and equal attenuation in all propagation paths, the measurement relation in (7) simplifies to

$$\bar{\boldsymbol{y}} = \left(\boldsymbol{A}^{(0)} + \boldsymbol{A}^{(1)} + \cdots + \boldsymbol{A}^{(K-1)}\right)\boldsymbol{s} = \bar{\boldsymbol{A}}\boldsymbol{s} \quad (8)$$

where $\boldsymbol{s}$ is the common reflectivity vector.

Hence, the reconstruction problem simplifies to a simple CS reconstruction problem, as proposed in [8]. However, the above common vector assumption usually does not hold in practical scenarios, especially for complex-shaped targets, where the target RCS depends on the bistatic angle.

3.2. Group Sparse CS Reconstruction

Next, a practical approach is introduced, where the limitations of the aforementioned reconstruction scheme are overcome. The target RCS usually varies strongly with the bistatic angle; hence, we cannot assume prior knowledge of the exact relationship between the various sub-images $\boldsymbol{s}^{(k)}$. However, we know that all sub-images are representations of the same ground-truth. If a target location in one sub-image has non-zero reflectivity, this should also be the case for the corresponding location in all other sub-images. In other words, if a pixel is in the support of one sub-image, it should be in the support of all other sub-images. Hence, the K sub-images $\boldsymbol{s}^{(k)}$ share, at least approximately if not exactly, the same support. This observation calls for a group sparse or structured sparse reconstruction, which we describe below.

First, all unknowns in model (7) can be stacked to form one tall vector $\tilde{\boldsymbol{s}} = \left[\left(\boldsymbol{s}^{(0)}\right)^T \left(\boldsymbol{s}^{(1)}\right)^T \cdots \left(\boldsymbol{s}^{(K-1)}\right)^T\right]^T$. The measurements can then be expressed as

$$\bar{\boldsymbol{y}} = \tilde{\boldsymbol{A}}\tilde{\boldsymbol{s}}. \quad (9)$$

where the combined measurement matrix is obtained by concatenating the individual matrices into one fat matrix $\tilde{\boldsymbol{A}} = [\boldsymbol{A}^{(0)}\ \boldsymbol{A}^{(1)}\ \cdots\ \boldsymbol{A}^{(K-1)}]$.

The above high-dimensional model (9) is the basis for formulating the reconstruction problem using group sparse regularization. We choose ℓ_1 minimization using a mixed $\ell_1 - \ell_2$ norm regularization, as this approach promotes group sparse solutions [18, 19]. Hence, we obtain an optimization problem,

$$\hat{\tilde{\boldsymbol{s}}} = \arg\min_{\tilde{\boldsymbol{s}}} \frac{1}{2}\|\bar{\boldsymbol{y}} - \tilde{\boldsymbol{A}}\tilde{\boldsymbol{s}}\|_2^2 + \lambda\|\tilde{\boldsymbol{s}}\|_{2,1}, \quad (10)$$

where

$$\|\tilde{\boldsymbol{s}}\|_{2,1} := \sum_{p=0}^{N_x N_y - 1} \left\| \left[s_p^{(0)}, s_p^{(1)}, \ldots, s_p^{(K-1)}\right]^T \right\|_2 \quad (11)$$

and $\lambda > 0$ is the so-called regularization parameter. Problem (10) can be solved using SparSA [18]. By imposing a group-sparse constraint on the solution, the K-fold increase in the number of unknowns can be remedied and less measurements are required to obtain a unique solution.

In order to exploit the power received through multi-path propagation, the sub-images have to be combined to obtain a single composite image. As we do not know the phase of the individual reflectivities $s_p^{(k)}$, we resort to non-coherent combination of the sub-images. That is, we calculate the ℓ_2 norm across the pixels of the sub-images, $[\hat{\boldsymbol{s}}]_p = \left\| \left[\hat{s}_p^{(0)}, \hat{s}_p^{(1)}, \ldots, \hat{s}_p^{(K-1)}\right]^T \right\|_2$. This approach will not lead to improved signal-to-noise ratio in the presence of spatially white noise in the sub-images. However, we are able to improve the signal-to-clutter ratio. The returned power of a target is accumulated over all propagation paths. The remaining clutter, which is spatially non-white, will likely not be accumulated in a single location, and hence it is attenuated with respect to the target return.

4. RESULTS

For the simulation results, a 77-element uniform linear monostatic array with an inter-element spacing of 1.9 cm is used for imaging. The origin of the coordinate system is chosen to be at the center of the array. The concrete front wall is located parallel to the array at 2 m downrange and has a thickness $d = 20$ cm and relative permittivity $\epsilon = 7.67$. We consider three interior walls; the left and right side walls are located at ± 2 m crossrange while the back wall is at 5 m downrange. A stepped-frequency signal, consisting of 801 equally spaced

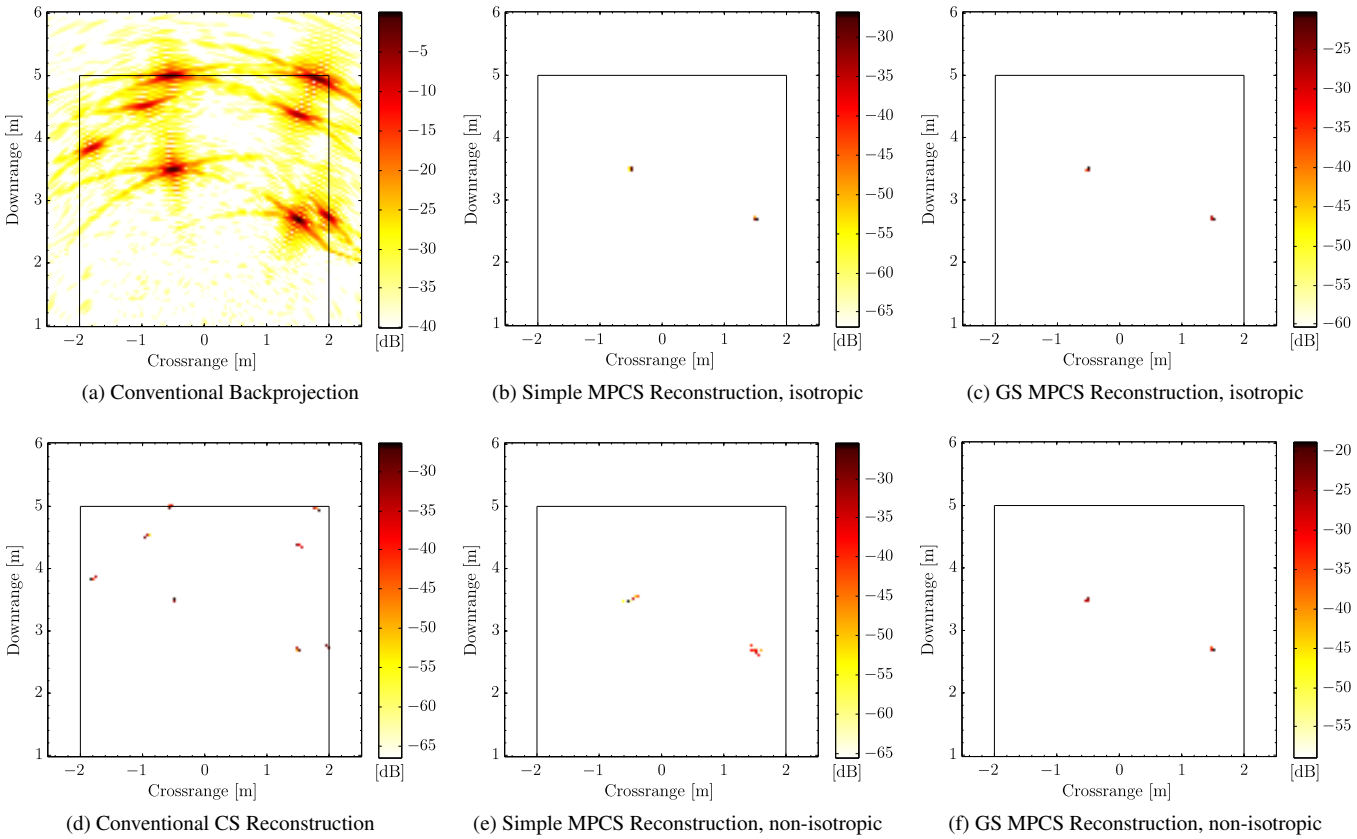

(a) Conventional Backprojection (b) Simple MPCS Reconstruction, isotropic (c) GS MPCS Reconstruction, isotropic

(d) Conventional CS Reconstruction (e) Simple MPCS Reconstruction, non-isotropic (f) GS MPCS Reconstruction, non-isotropic

Fig. 2. Backprojected image using the full data (a) along with various CS reconstruction results using one fourth of the array elements and on eights of the frequency bins (b-f).

frequency steps, covering the 1 to 3 GHz band, is employed for scene interrogation. We assume that all wall reflections have been properly suppressed and only the target signal remains.

We simulate two point targets, located at (1.5, 2.7) m and (-0.5, 3.5) m. In the received signal, the direct return along with multipath returns via the three interior walls are considered; hence, $K = 4$. Two different scenarios are simulated. In the first case, all targets are perfectly isotropic, resulting in equal reflectivity vectors $\boldsymbol{s}^{(k)}, k = 0, \ldots, K-1$. In the second case, we introduce a random phase shift for each target / multipath pair, which should simulate non-isotropic targets. However, for the sake of simplicity and comparability, we do not account for differences in the propagation losses of the paths. White Gaussian noise with 0 dB SNR is added to the simulated measurements. For comparison, the backprojected image using the full data record is depicted in Fig. 2a. For the proposed CS reconstructions, we use one-fourth of the array elements and one-eighth of the frequencies. The corresponding results, averaged over 100 Monte Carlo runs, are depicted in Figs. 2(b)-(f).

Conventional CS reconstruction of the image, without taking multipath propagation into consideration, does not lead to good results. The targets are reconstructed along with all the ghosts, leading to an ambiguous interpretation of the scene, see Fig. 2(d). In the isotropic target scenario, both the simple and the group sparse (GS) multipath CS (MPCS) reconstruction algorithms are able to reconstruct the two targets perfectly, refer to Figs. 2(b),(c). All ghost targets are reliably suppressed. However, if we consider non-isotropic targets, the group sparse approach clearly outperforms the simple MPCS approach, as depicted in Figs. 2(e),(f). Due to the inaccurate measurement model in the simple MPCS, the point targets become weaker and cannot be accurately located. Clearly, the group sparse approach does not suffer from such problems.

5. CONCLUSION

Based on a multipath propagation model for TWRI, we have proposed group sparse reconstruction approaches under efficient data collection towards the objective of reconstructing the ground truth of the image without multipath ghosts. Results based on simulated data have shown good reconstructions, featuring a clean image with suppressed ghosts.

6. REFERENCES

[1] F. Ahmad and M.G. Amin, "Multi-location wideband synthetic aperture imaging for urban sensing applications," *Journal of the Franklin Institute*, vol. 345, no. 6, pp. 618 – 639, September 2008.

[2] E.J. Baranoski, "Through-wall imaging: Historical perspective and future directions," *Journal of the Franklin Institute*, vol. 345, no. 6, pp. 556 – 569, September 2008.

[3] F. Ahmad, M.G. Amin, and P.D. Zemany, "Dual-frequency radars for target localization in urban sensing," *IEEE Transactions on Aerospace and Electronic Systems*, vol. 45, no. 4, pp. 1598 –1609, oct. 2009.

[4] M.G. Amin, Ed., *Through-the-Wall Radar Imaging*, CRC Press, 2010.

[5] M.G. Amin and F. Ahmad, "Wideband synthetic aperture beamforming for through-the-wall imaging [lecture notes]," *IEEE Signal Processing Magazine*, vol. 25, no. 4, pp. 110 –113, july 2008.

[6] P. Setlur, M. Amin, and F. Ahmad, "Multipath model and exploitation in through-the-wall and urban radar sensing," *IEEE Transactions on Geoscience and Remote Sensing*, vol. 49, no. 10, pp. 4021–4034, 2011.

[7] S. Kidera, T. Sakamoto, and T. Sato, "Extended imaging algorithm based on aperture synthesis with double-scattered waves for UWB radars," *IEEE Transactions on Geoscience and Remote Sensing*, vol. 49, no. 12, pp. 5128 – 5139, 2011.

[8] Y.-S. Yoon and M.G. Amin, "Compressed sensing technique for high-resolution radar imaging," in *Proceedings of SPIE*, 2008, vol. 6968, p. 69681A.

[9] F. Ahmad and M. G. Amin, "Through-the-wall human motion indication using sparsity-driven change detection," *IEEE Transactions on Geoscience and Remote Sensing*, vol. 51, no. 2, pp. 881 –890, feb. 2013.

[10] M. Leigsnering, C. Debes, and A.M. Zoubir, "Compressive sensing in through-the-wall radar imaging," in *IEEE International Conference on Acoustics, Speech and Signal Processing*, May 2011.

[11] F. Ahmad, Ed., *Compressive Sensing*, vol. 8365 of *Proceedings of SPIE*, Bellingham, WA, 2012. SPIE.

[12] M. Leigsnering, A.M. Zoubir, F. Ahmad, and M.G. Amin, "Multipath exploitation in through-the-wall radar imaging using sparse reconstruction," *IEEE Transactions on Aerospace and Electronic Systems*, 2012, Submitted for publication.

[13] E. L. Targarona, M. G. Amin, F. Ahmad, and M. Nájar, "Wall mitigation techniques for indoor sensing within the cs framework," in *Proc. Seventh IEEE workshop on sensor array and multi-channel signal processing*, 2012.

[14] F. H. C. Tivive, M. G. Amin, and A. Bouzerdoum, "Wall clutter mitigation based on eigen-analysis in through-the-wall radar imaging," in *Proc. 17th Int Digital Signal Processing (DSP) Conf*, 2011, pp. 1–8.

[15] Y.-S. Yoon and M.G. Amin, "Spatial filtering for wall-clutter mitigation in through-the-wall radar imaging," *IEEE Transactions on Geoscience and Remote Sensing*, vol. 47, no. 9, pp. 3192 –3208, Sept. 2009.

[16] C. Thajudeen, A. Hoorfar, and Wenji Zhang, "Estimation of frequency-dependent parameters of unknown walls for enhanced through-the-wall imaging," in *IEEE International Symposium on Antennas and Propagation (APSURSI)*, july 2011, pp. 3070 –3073.

[17] A.C. Gurbuz, J.H. McClellan, and W.R. Scott, "A compressive sensing data acquisition and imaging method for stepped frequency GPRs," *IEEE Transactions on Signal Processing*, vol. 57, no. 7, pp. 2640 –2650, July 2009.

[18] S.J. Wright, R.D. Nowak, and M.A.T. Figueiredo, "Sparse reconstruction by separable approximation," *IEEE Transactions on Signal Processing*, vol. 57, no. 7, pp. 2479–2493, 2009.

[19] R.G. Baraniuk, V. Cevher, M.F. Duarte, and Chinmay Hegde, "Model-based compressive sensing," *IEEE Transactions on Information Theory*, vol. 56, pp. 1982–2001, April 2010.